REPORT DOCUMENTATION PAGE

Form Approved OMB NO. 0704-0188

1. REPORT DATE (DD-MM-YYYY)	2. REPORT TYPE	3. DATES COVERED (From - To)
17-01-2015	Conference Proceeding	-

4. TITLE AND SUBTITLE
DESIGN AND TEST OF A TRANSONIC AXIAL SPLITTERED ROTOR

5a. CONTRACT NUMBER

5b. GRANT NUMBER
ARO MI-PR--

5c. PROGRAM ELEMENT NUMBER
611102

6. AUTHORS
Garth Hobson, PhD, Anthony Gannon, PhD, Scott Drayton, LCDR USN

5d. PROJECT NUMBER

5e. TASK NUMBER

5f. WORK UNIT NUMBER

7. PERFORMING ORGANIZATION NAMES AND ADDRESSES
Naval Postgraduate School (NPS-Monterey) 14,973.00
1 University Circle
Monterey, CA 93943 -5000

8. PERFORMING ORGANIZATION REPORT NUMBER

9. SPONSORING/MONITORING AGENCY NAME(S) AND ADDRESS (ES)
U.S. Army Research Office
P.O. Box 12211
Research Triangle Park, NC 27709-2211

10. SPONSOR/MONITOR'S ACRONYM(S)
ARO

11. SPONSOR/MONITOR'S REPORT NUMBER(S)
60039-EG.3

12. DISTRIBUTION AVAILIBILITY STATEMENT
Approved for public release; distribution is unlimited.

13. SUPPLEMENTARY NOTES
The views, opinions and/or findings contained in this report are those of the author(s) and should not contrued as an official Department of the Army position, policy or decision, unless so designated by other documentation.

14. ABSTRACT
A new design procedure was developed that uses commercial-off-the-shelf software (MATLAB, SolidWorks, and ANSYS-CFX) for the geometric rendering and analysis of a transonic axial compressor rotor with splitter blades. Predictive numerical simulations were conducted and experimental data were collected in a Transonic Compressor

15. SUBJECT TERMS
Transonic Axial Compressor, Splittered Rotor

16. SECURITY CLASSIFICATION OF:			17. LIMITATION OF ABSTRACT	15. NUMBER OF PAGES	19a. NAME OF RESPONSIBLE PERSON
a. REPORT	b. ABSTRACT	c. THIS PAGE			Garth Hobson
UU	UU	UU	UU		19b. TELEPHONE NUMBER 831-656-2888

Report Title

DESIGN AND TEST OF A TRANSONIC AXIAL SPLITTERED ROTOR

ABSTRACT

A new design procedure was developed that uses commercial-off-the-shelf software (MATLAB, SolidWorks, and ANSYS-CFX) for the geometric rendering and analysis of a transonic axial compressor rotor with splitter blades. Predictive numerical simulations were conducted and experimental data were collected in a Transonic Compressor Rig. This study advanced the understanding of splitter blade geometry, placement, and performance benefits. In particular, it was determined that moving the splitter blade forward in the passage between the main blades, which was a departure from the trends demonstrated in the few available previous transonic axial compressor splitter blade studies, increased the mass flow range with no loss in overall performance. With a large 0.91 mm (0.036 in) tip clearance, to preserve the integrity of the rotor, the experimentally measured peak total-to-total pressure ratio was 1.69 and the peak total-to-total isentropic efficiency was 72 percent at 100 percent design speed. Additionally, a higher than predicted 7.5 percent mass flow rate range was experimentally measured, which would make for easier engine control if this concept were to be included in an actual gas turbine engine.

Conference Name: ASME TURBO Expo 2015

Conference Date: June 15, 2015

Proceedings of TURBO EXPO 2015:
ASME TURBO EXPO 2015: Land, Sea and Air
June 2015, Montreal, Canada

GT2015-43005

DESIGN AND TEST OF A TRANSONIC AXIAL SPLITTERED ROTOR

Garth V. Hobson
Naval Postgraduate School
Monterey, CA, USA

Anthony J. Gannon
Naval Postgraduate School
Monterey, CA, USA

Scott Drayton
United States Naval Academy
Annapolis, MD, USA

ABSTRACT

A new design procedure was developed that uses commercial-off-the-shelf software (MATLAB, SolidWorks, and ANSYS-CFX) for the geometric rendering and analysis of a transonic axial compressor rotor with splitter blades. Predictive numerical simulations were conducted and experimental data were collected in a Transonic Compressor Rig. This study advanced the understanding of splitter blade geometry, placement, and performance benefits. In particular, it was determined that moving the splitter blade forward in the passage between the main blades, which was a departure from the trends demonstrated in the few available previous transonic axial compressor splitter blade studies, increased the mass flow range with no loss in overall performance. With a large 0.91 mm (0.036 in) tip clearance, to preserve the integrity of the rotor, the experimentally measured peak total-to-total pressure ratio was 1.69 and the peak total-to-total isentropic efficiency was 72 percent at 100 percent design speed. Additionally, a higher than predicted 7.5 percent mass flow rate range was experimentally measured, which would make for easier engine control if this concept were to be included in an actual gas turbine engine.

.

INTRODUCTION

Over the course of turbomachinery development splitter vanes have been used extensively in centrifugal compressors. Axial compressor rotors with splitter blades have been studied and shown potential for producing desirable performance characteristics (high stage pressure ratios and efficiencies), but have failed to gain traction due to perceived negative performance characteristics such as narrow mass flow operating ranges. According to Wennerstrom [1];

"Starting in the late 1980s, three different engine companies have explored the concept with contemporary CFD tools and have tested some prototypes. Some of these results showed great promise. None of this work has been published openly yet, but this approach does appear to offer prospects for good diffusion factors on the order of 0.5 to 0.7 and possibly higher. The key to successful application will be the development of a splitter-vane design procedure that balances and optimizes the pressure distributions in the two passages created by the splitter vane. An important component of this will be a viscous CFD code that handles shock waves, high diffusion, and separated regions well."

Starting in 1971, Wennerstrom [2-5] and co-workers at the Fluid Dynamics Research Laboratory, Aerospace Research Laboratories, Wright-Patterson Air Force Base, Ohio designed and tested a variant of a supersonic axial compressor stage that incorporated splitter vanes in the aft section of the rotor passage. This study resulted in a rotor that contained 30 main blades and 30 splitter blades depicted in Fig 1. The splitter blade camber line duplicated the camber line of the main blades and was circumferentially positioned exactly midway between main blades. The splitter blades extended the full radial span and their leading edges were placed halfway between the inlet and exit planes of the rotor. Additionally, the trailing edges of the splitter blades were in the same axial plane as the trailing edges of the main blades as shown in Fig 2. At 100 percent design speed, Wennerstrom's rotor achieved an experimentally measured peak total-to-total pressure ratio of 3.36 and a

peak total-to-total isentropic efficiency of 84 percent. Detracting from these impressive results was a very narrow mass flow rate range of 3 percent.

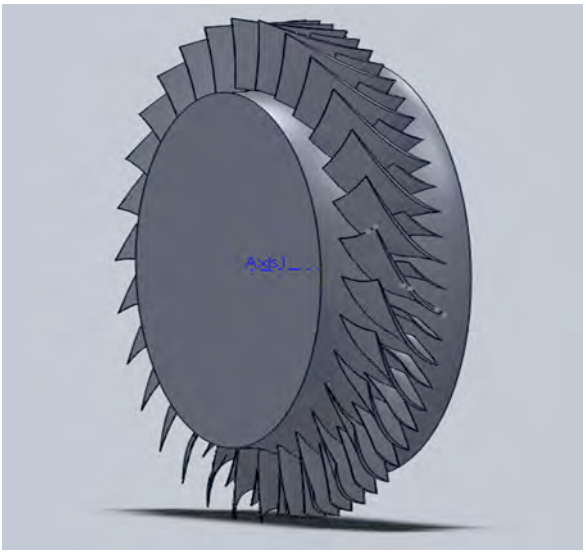

Fig. 1, Wennerstrom and Hearsey transonic axial compressor splittered rotor [3].

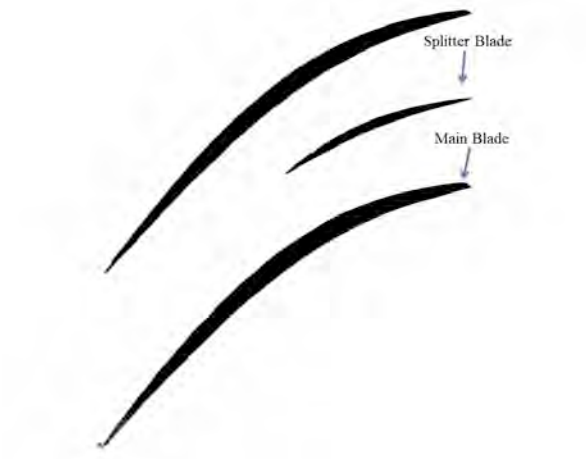

Fig. 2, Wennerstrom and Hearsey tip section [3].

Tzuoo, et al. [6] revisited Wennerstrom's work and developed a design methodology that combined a meridional flow calculation, an arbitrary blading design procedure, and 3-d inviscid and viscous analyses. Their methodology advanced the overall design approach of splittered axial compressor rotors and was demonstrated via analyses of Wennerstrom's splittered rotor showing the importance of 3-d viscous effects.

McClumphy [7] focused on the numerical analysis of tandem airfoils in the rear stages of a core axial-flow compressor in subsonic conditions. This work advanced the understanding of tandem rotor fluid mechanics providing a better understanding of forward and aft blade behavior.

This study revisited axial compressor rotors with splitter blades by the design, build, test, and evaluation of a non-axisymmetric rotor with splitter blades that retain the positive performance characteristics while addressing the previously identified deficiencies. Axial compressor rotors with splitter blades will be desirable in large commercial and military engines and smaller gas turbine applications such as helicopters and unmanned aerial vehicles.

NOMENCLATURE

c	-	Absolute velocity
C_p	-	Specific heat
HP_C	-	Power
M	-	Mach number
$\dot{m}$	-	Corrected mass flow rate ($=\dot{m}\sqrt{\theta}/\delta$)
T	-	Temperature
U	-	Blade speed
W	-	Specific Weight Flow
w	-	Relative Velocity

Greek Symbol

δ	-	Referred pressure
γ	-	Ratio of Specific Heats
η	-	Isentropic Efficiency
θ	-	Referred temperature

Subscript

0	-	Stagnation
1	-	Upstream
2,3	-	Downstream
rel	-	Relative
tip	-	Tip
z	-	Axial direction

List of Abbreviation

AR	-	Aspect Ratio
AS	-	Axial Station
AVR	-	Axial Velocity Ratio
CFD	-	Computational Fluid Dynamics
HER	-	Hub Exit Radius
LE	-	Leading Edge
MB	-	Main Blade
PR	-	Pressure Ratio
PS	-	Pressure Side
SA	-	Stagger Angle
SB	-	Splitter Blade
SS	-	Suction Side
TASR	-	Transonic Axial Splitter Rotor
TCR	-	Transonic Compressor Rig
TER	-	Tip Exit Radius
TG	-	Tip Gap
TIR	-	Tip Inlet Radius
TPL	-	Turbopropulsion Laboratory

DESIGN TOOLS AND PROCEDURE

Adaptation of Sanger Preliminary Design Method

In the 1990s, a transonic axial rotor–stator stage was designed by Nelson L. Sanger of NASA Lewis Research Center exclusively for the Naval Postgraduate School as a research and teaching tool. Sanger's transonic axial compressor rotor is shown in Fig 3. The design process and methodology followed is documented in Sanger [8, 9], which resulted in a low aspect ratio (1.2) rotor with a tip relative inlet Mach number of 1.3, and an overall stage pressure ratio of 1.57. Over the course of approximately ten years experimental and numerical investigations evaluated the Sanger compressor performance over a variety of operating speeds and conditions.

Fig. 3, Sanger's transonic axial compressor rotor [14].

Having proven that the Sanger design methodology was robust by extensive performance evaluation, parts of his work were adapted as a starting point for the design portion of this study. The preliminary design steps, which he followed and documented in detail [9], were coded in a MATLAB script. Initially the Sanger method required ambient conditions, gas properties and the input design parameters such as stagnation pressure ratio (PR), efficiency (η), aspect ratio (AR), stagger angle (SA), specific weight flow (W), axial velocity ratio (AVR), inlet and exit tip radii and the exit hub radius (TIR, TER and HER).

To provide a more accurate estimate of the blade angles required to start the design process for the transonic conditions of the splitter rotor passage, a normal shock was assumed to be situated in the passage as shown in Fig 4.

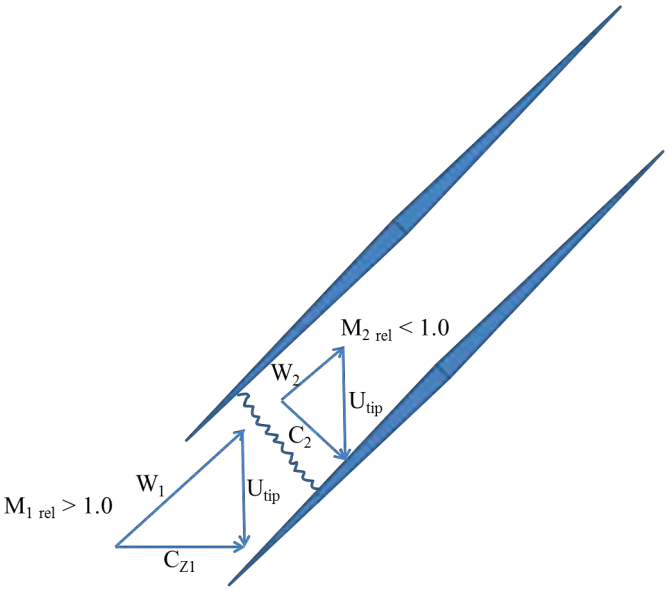

Fig. 4, Loss model based on a single normal shock in passage.

Calculations to construct the inlet velocity triangle were completed using the blade tip Mach number calculated earlier using the Sanger method. Starting with the inlet relative Mach number at the tip as well as the specified AVR, a normal shock wave was computed using equation (1) to determine the downstream relative subsonic Mach number and associated velocity (W_2) shown in Fig 5.

$$M^2_{2rel} = \frac{M^2_{1rel} + \frac{2}{\gamma - 1}}{\left(\frac{2\gamma}{\gamma - 1}\right)\left(M^2_{1rel} - 1\right)} \qquad (1)$$

The inlet and outlet velocity triangles are combined to show the net turning resulting from a normal shock located in the rotor passage. The combined velocity triangle with an AVR of 0.90 is shown in Fig 5, after subsonic turning of the flow aft of the shock.

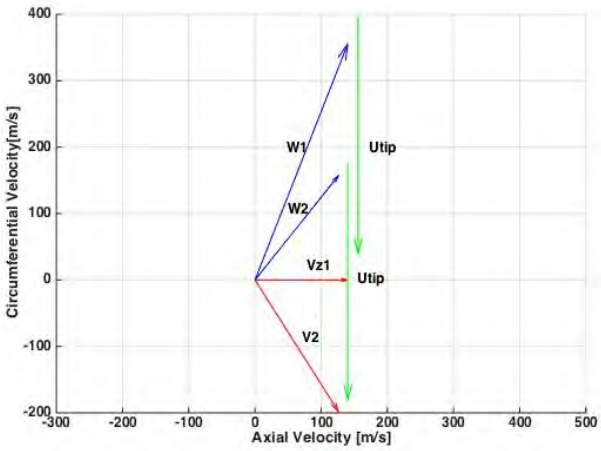

Fig. 5, Rotor tip section combined velocity triangles.

Automation

Recent computational fluid dynamics (CFD) studies at the Turbopropulsion Laboratory (TPL) have made extensive use of SolidWorks, a commercial solid modeling program, and ANSYS Workbench, a commercial simulation package that includes amongst others mesh generation, structural analysis, modal analysis, and CFD modules. The gas path analysis methods used in those previous studies are well documented in Boyter [11] and McNab [12]. Rotor gas path solid models were developed in SolidWorks and then imported into ANSYS CFX for performance analysis. The interface between SolidWorks and ANSYS required manual intervention. Any changes to the rotor gas path solid model required human-in-the-loop modification followed by manual updating of ANSYS Design Modeler and refreshing of ANSYS CFX setup for performance analysis. Additionally, to predict the data required to produce a rotor performance map, throttling needed to occur via manual manipulation of the rotor gas path outlet pressure.

Given this study's objectives and time constraints, it was apparent a design tool that automated geometry generation and CFD analysis as well as the interface between the standalone commercial software packages SolidWorks and ANSYS was required. MathWorks' MATLAB technical computing language was chosen as the software package to interface with SolidWorks and ANSYS Workbench. Versions MATLAB R2012b, SolidWorks 2010, and ANSYS Workbench 14.0 were used in this study. The resultant design tool process flow chart is shown in Fig 6.

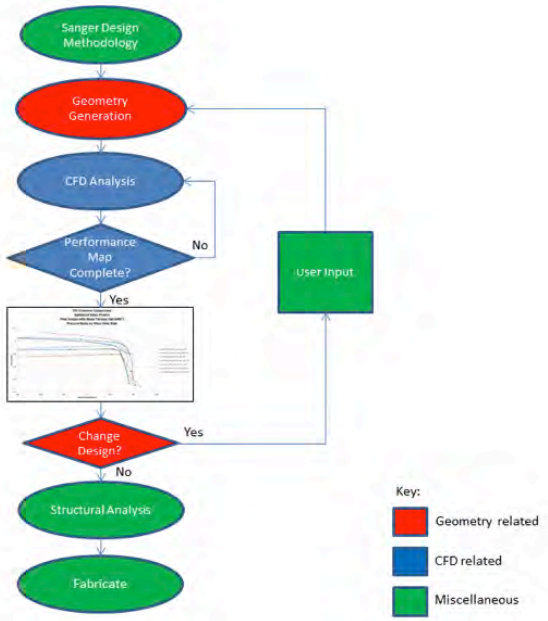

Fig. 6, Design process flow chart.

Geometry Generation

To begin the design process, the Sanger design methodology with the incorporated shock loss model was used to produce inlet and outlet velocity triangles. From these velocity triangles, overall stage flow turning angles were calculated and used to guide the user inputs for blade angles and thickness distributions. Armed with basic blade geometry parameters the TPL design tool was initiated by running the MATLAB script (*.m) Main_SpeedLine_Auto. Main_SpeedLine_Auto called the following MATLAB scripts:

- HardCodeBlade
- HardCodeParams
- GeomGen
- FluidAnalysis
- ArchiveRunData
- WriteSpreadsheet

These MATLAB scripts will now be discussed. The HardCodeBlade script was responsible for loading all main and splitter blade user customizable parameters into Main_Speedline_Auto.

Table 1. HardCodeBlade Parameters

Input Parameter Description	Input Parameter
	Blade.PassNo
No. of spanwise blade sections	Blade.S
No. of pts. that define blade profile	Blade.P
Blade heights at which properties are inputted	Blade.Heights
Blade chords at prescribed blade heights	Blade.Chord
Blade leading edge shift as a fraction of axial chord at prescribed blade heights	Blade.LE
Blade leading and trailing edge ellipse characteristics (minor axis/chord, eccentricity).	Blade.Edges
Blade chord control locations	Blade.Controls
Blade stagger at prescribed blade heights and blade chord control locations	Blade.Stagger
Blade element thickness at prescribed blade heights AND blade chord control locations	Blade.Thickness
Blade offset representing the fraction of the passage to rotate each blade element (Main blades at 0.0)	Blade.Offset
Blade axial shift for all blades	Blade.MasterXShift
Fillet radius of all blades	Blade.Fillet
Centering feature (Boolean) specifying whether to center the main blade on the hub origin (true) or align the main blade leading edge with the origin (false) before applying the prescribed axial shift	Blade.Center

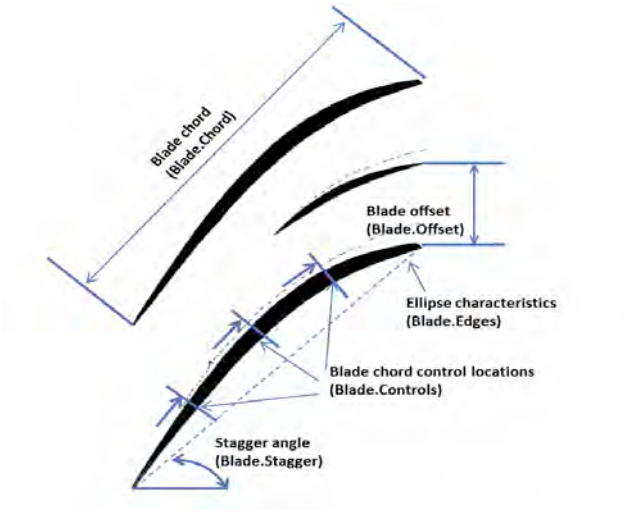

Fig. 7, HardCodeBlade blade input parameters.

Some of the blade input parameters and passage input parameters listed in Table 1 are shown in Fig 7 and Fig 8 respectively.

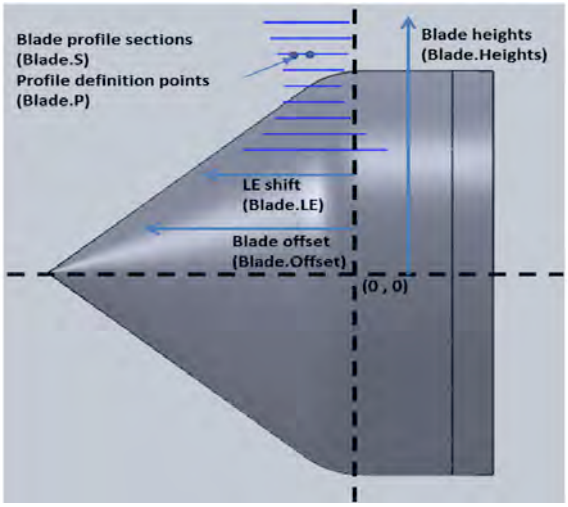

Fig. 8, HardCodeBlade passage input parameters.

The HardCodeParams script was responsible for loading the ambient conditions, gas properties, and the other constants and parameters associated with the overall geometry such as inlet and exit, casing and hub radii.

The GeomGen script was the main routine responsible for blade, hub, spinner, and casing geometry generation and rotor and air wedge solid model generation in SolidWorks. To accomplish this GeomGen called the following seven MATLAB scripts:

- BladeGen
- SangerMethod
- Passage
- WedgeGen
- StreamGen
- SolidWorksGen
- BladeHub_Wedge_CutOut

Using the parameters passed in and described above, bladegen started the blade profile generation process by calling the bladesect script. Depending on the number of blade sections prescribed earlier, bladegen generated blade sections by repeatedly calling bladesect for both the main blade and splitter blade. Bladesect used a third-order spline between control points for camber line distribution as shown in Fig 9.

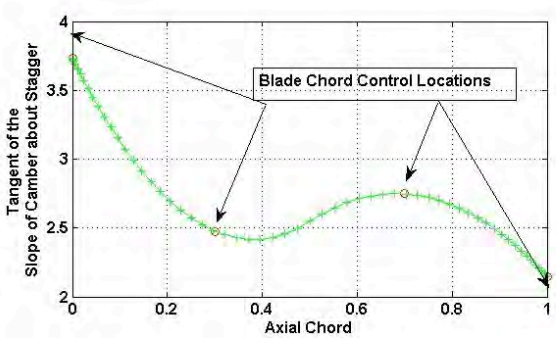

Fig. 9, Third-order spline fit for blade camber line distribution

Blade profile generation continued by using a third-order spline between control points for thickness distribution as shown in Fig 10. The red lines denoting the leading edge and trailing edge blend points.

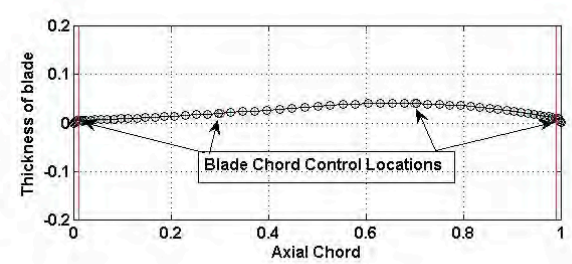

Fig. 10, Third-order spline fit for blade thickness distribution.

A magnification of Fig 10 at the blade leading edge which shows the blend point between the third order spline on the blade and the ellipse of the leading edge is shown in Fig 11.

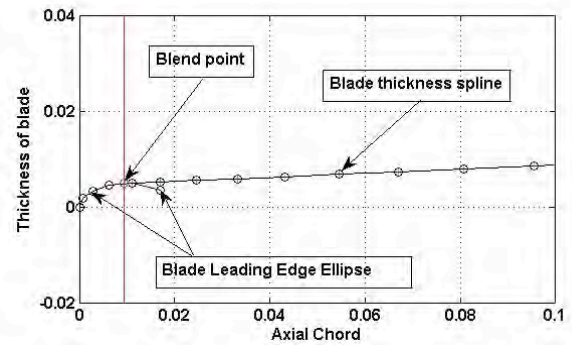

Fig. 11, Blade leading edge: third-order spline fit for thickness.

The thickness distribution accounted for the user-defined blade leading edge and trailing edge ellipse dimensions and eccentricity. Additionally it also ensured blending to the blade surface by matching slopes at corresponding transition points as shown in Fig 12.

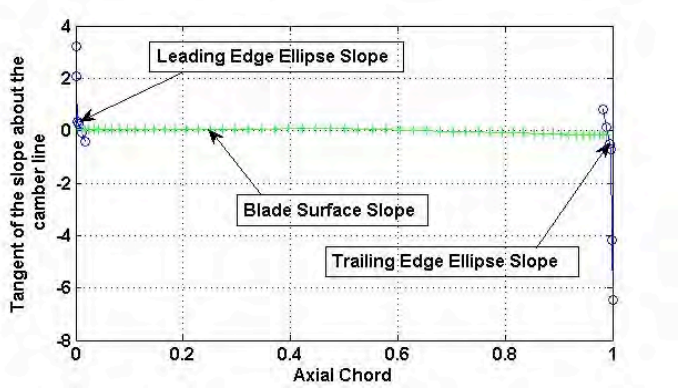

Fig. 12, Blade leading edge and trailing edge slope blending.

Each blade section generated within BladeSect was stacked on its centroid by using the values passed from the polygeom MATLAB script. The polygeom script was derived from Sommer [14] and generated properties (area, x-centroid, y-centroid, perimeter, and area moments of inertia) of a planar polygon. These blade profiles were then passed to SolidWorks for solid model generation of the blade shapes.

With all required blade section geometries generated, GeomGen then used the SangerMethod, Passage, and WedgeGen MATLAB scripts to generate spinner, hub, passage and air wedge geometries. GeomGen then called MATLAB script StreamGen to calculate streamline radial positions with assistance from the following MATLAB scripts:

- d-d which utilized a numerical method to find the first derivative of two variables.
- NEWS which found the north, south, east, and west points of a non-uniform grid.
- extrap which performed quadratic extrapolation on three internal points to fit a quadratic polynomial in order to find the edge point.

With all required geometries and streamline data computed, GeomGen then called MATLAB script SolidWorksGen which sent commands to SolidWorks to generate a solid model of the full air wedge. This was accomplished by modifying the existing SolidWorks part files (*.SLDPRT) BasicRotor and BasicWedge with the geometry and streamline data generated earlier. Via its interface with SolidWorks, SolidWorksGen produced the solid models listed in Table 2.

Table 2 SolidWorksGen Solid Models

Solid Model	Description
BladeHub_Full	Complete rotor
BladeHub_Wedge_Cutout	Portion of rotor contained within a one-passage air wedge
AirWedge	One-passage air wedge without blade fillets
AirWedge_Fillets	One-passage air wedge with blade fillets
AirWedge_Upstream	Portion of one-passage air wedge removed upstream of rotor inlet area to reduce computational domain
AirWedge_Downstream	Portion of one-passage air wedge removed downstream of rotor exit area to reduce computational domain

All these solid models were saved as Parasolid (*.x_t) and SolidWorks (*.SLDPRT) files, which could then be used for CFD and structural/modal analyses.

Computational Analysis Setup

With solid models generated of the gas-path air wedge, automated numerical performance analysis using CFX within ANSYS Workbench was performed. This was desired in order to produce the data required to generate rotor performance maps. Main_Speedline_Auto continued operation by calling the MATLAB script FluidAnalysis to produce a single speed line from open throttle (zero back pressure) to near stall. FluidAnalysis completed the following calls:

- WorkingProject.
- UpdateProject1 or UpdateProject2
- ReadAnsysData

The automation terminated when on the current simulation the parameter of interest (pressure ratio, efficiency or power) specified in Main_Speedline_Auto was below the same parameter on the previous simulation or was not a valid number. The cumulative data stored in the spreadsheet was used to map rotor performance graphically.

The computational domain, as shown in Fig 13, extended three axial chord lengths upstream of the rotor (one chord length upstream of the spinner) and two axial chord lengths aft of the rotor. All the design analysis runs were carried out with zero tip gap (TG) and the computational mesh for a single passage had 1.6 million nodes (or 7.2 million elements). Prismatic elements were used as inflation layers on the blade surfaces for 9 layers with a 1.2 stretching factor off the surface. The standard k-epsilon turbulence model was used through out as were high-speed numeric and compressibility corrections to account for correct shock resolution.

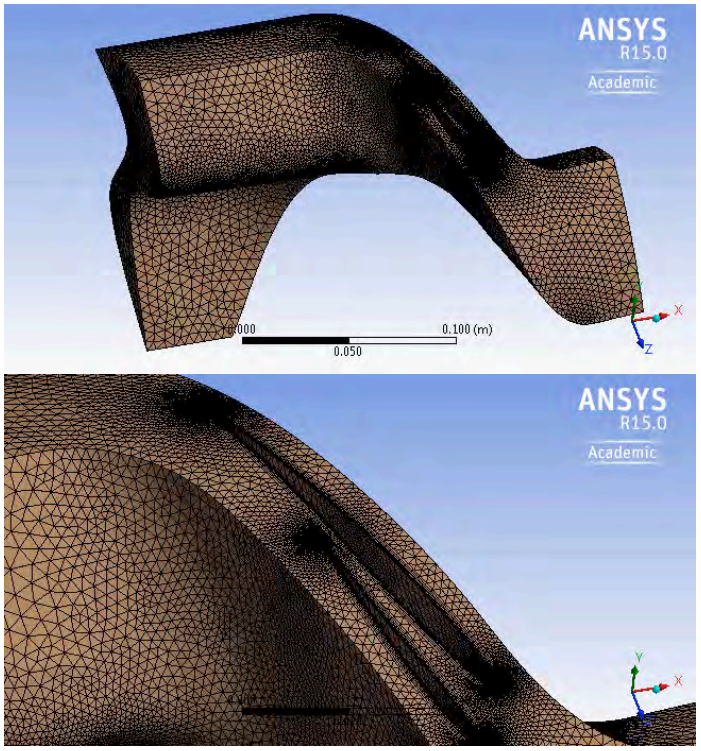

Fig. 13, Design sequence computational domain.

Minimum flow rates were determined when either of the following occurred during the simulation;

(1) less than three orders of magnitude convergence of the residuals
(2) marked drop off of the efficiency
(3) marked drop off of the mass flow rate

Regardless, user interface was still needed to determine three predicted operating range by polling all three of the criteria.

DESIGN OF A TRANSONIC AXIAL COMPRESSOR ROTOR WITH SPLITTER BLADES

The constraints and goals for the Transonic Axial Splittered Rotor (TASR) are listed in Table 3. Additionally a specific weight flow of 195 kg/s-m^2 (40 lbm/s-ft^2) or a mass flow rate of 5.5 kg/sec was targeted.

Table 3. TASR Design Constraints and Goals

Parameter	Goal	Constraint
Rotor Input Power	500 kW	Constrained by available TCR drive turbine output power
Outlet Total-to-Inlet Total Pressure Ratio	1.8 : 1	None
Outlet Total-to-Inlet Total Isentropic Efficiency	80%	None
100% rotor speed	27,000 rpm	None
Casing Diameter	287 mm (11.3 in)	Constrained by existing TCR geometry
Number of Passages	12	None

A blade tip-down design approach was used. The outputs of the previously described combined Sanger method and shock-loss model were used as the starting inputs for the design process. These served as the starting point for good practice human-in-the-loop design improvement.

Four major designs, referred to as Baseline and Spirals 1–3, were explored during the course of the design process and are listed in Table 4. Several iterations were made within each major design study and performance maps for each design and iteration at 100 percent speed (27,000 RPM) were constructed.

The baseline design was derived from the outputs of the combined Sanger method and shock-loss model. The Baseline design solid model was inputted to the Fluid Flow (CFX) module and a mesh was created using Mechanical Model in ANSYS Workbench. The numerically derived total-to-total pressure ratio versus mass flow rate performance map is shown in Fig 14. At 100 percent design speed the predicted peak total-to-total peak pressure ratio was 1.65. The numerically derived total-to-total isentropic efficiency versus mass flow rate performance map is shown in Fig 15. At 100 percent design speed the predicted peak efficiency was 84.9 percent. Those results did not meet the TASR pressure ratio goal outlined in Table 3.

Additionally, it was decided that the splitter blade's chord was too long and it resembled a main blade. To ensure the design adhered to the SB concept developed by Wennerstrom [2] a new design constraint was implemented: the SB chord was limited to 50 percent or less of the MB chord.

Table 4. TASR Design Iterations

Design Iteration	Blade Profile	Splitter Blade Chord	Axial Blade Place-ment	Splitter Blade Passage Place-ment
Baseline	Baseline	Splitter blade (SB) chord > 50% main blade (MB) chord	0.00	50%
Spiral 1	Improved Baseline	SB chord = 50% MB chord	0.00	45%
Spiral 2	Improved Spiral 1	SB chord = 50% MB chord	-0.50 - +0.01	40%
Spiral 3	Spiral 2	SB chord = 50% MB chord	-0.02	30 – 35%

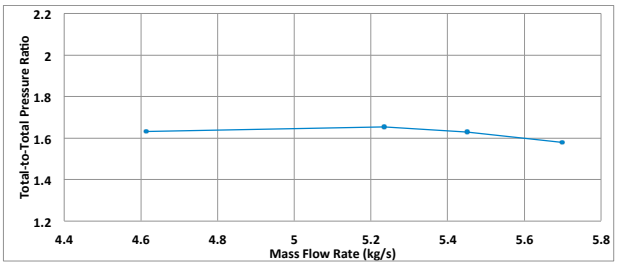

Fig. 14, TASR baseline: Total-to-total pressure ratio map.

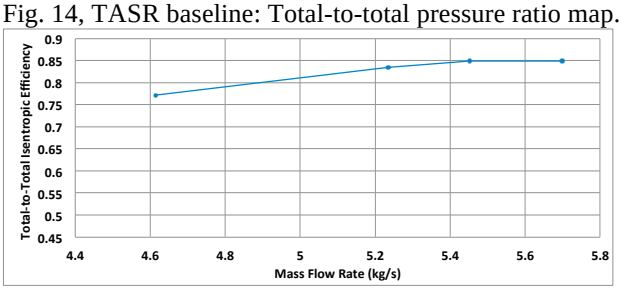

Fig. 15, TASR baseline: Isentropic efficiency map.

The Spiral 1 design implemented the new, self-imposed SB chord design constraint. To counteract the reduction in solidity caused by the shorter SB chord both the MB and SB chords were adjusted, the SB was moved from 50 percent circumferential passage placement (location between the pressure side (PS) and suction side (SS) of the two adjacent MBs) to 45 percent, and both blade profiles were improved. Iterations examined the performance impacts of increased chord lengths on both blades, forward sweep on the MB, and thinner MB and SB. At 100 percent design speed the predicted peak total-to-total pressure ratio was 1.70 and the predicted peak

total-to-total isentropic efficiency was 87.7 percent. These performance results also did not meet the TASR pressure ratio design goal outlined in Table 5 and the mass flow rate range was narrower than desired and intuition indicated performance improvements could be achieved by further blade geometry manipulation. The numerically derived total-to-total pressure ratio versus mass flow rate performance map is shown in Fig 16. The numerically derived total-to-total isentropic efficiency versus mass flow rate performance map is shown in Fig 17.

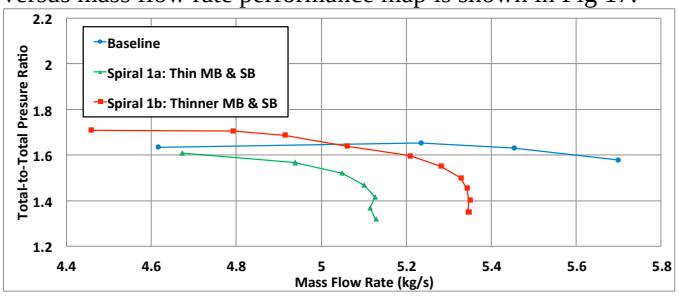

Fig. 16, TASR Spiral 1: Total-to-total pressure ratio map.

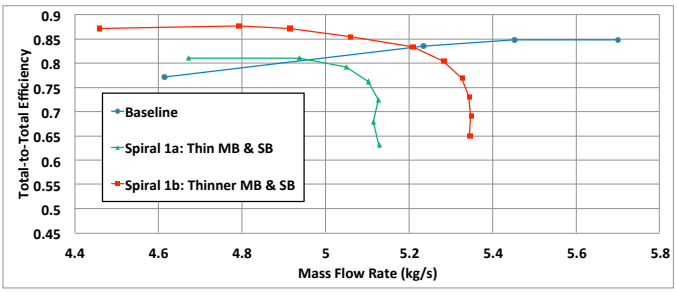

Fig. 17, TASR Spiral 1: Isentropic efficiency map.

The Spiral 2 design improved upon the Spiral 1 blade profile, retained the SB chord restriction, shifted the SB radial placement to 40 percent, and explored the performance impacts of moving the MB and SB axially forward and aft along the hub using the MATLAB script HardCodeBlade input parameter Blade.MasterXShift previously described in Table 1. Varying performance resulted from moving the blades forward and aft. The Spiral 2b design predicted peak total-to-total pressure ratio was 1.83 and the predicted peak total-to-total peak isentropic efficiency was 86.9 percent meeting the design goals of 1.8 and 80 percent respectively; however, the mass flow rate range was still too narrow. The numerically derived total-to-total pressure ratio versus mass flow rate performance map is shown in Fig 18. The numerically derived total-to-total isentropic efficiency versus mass flow rate performance map is shown in Fig 19.

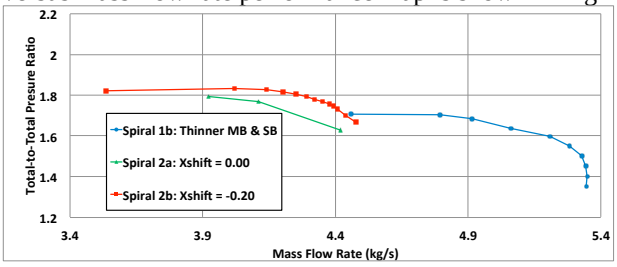

Fig. 18, TASR Spiral 2: Total-to-total pressure ratio map.

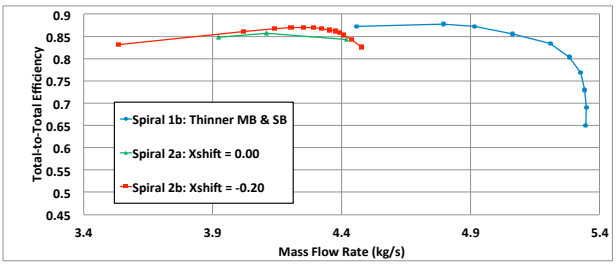

Fig. 19, TASR Spiral 2: Isentropic efficiency map.

The results of this axial blade placement study showed that with Blade.MasterXShift = -0.02 (forward) the rotor produced the best results. The Spiral 3 design froze the geometry of the Spiral 2b design and concentrated on exploring the performance impacts of moving the SB radially in the passage. Varying performance resulted from moving the SB radially between the adjacent MBs. The numerically derived total-to-total pressure ratio versus mass flow rate performance map is shown in Fig 20. The numerically derived total-to-total isentropic efficiency versus mass flow rate performance map is shown in Fig 21. The results of this SB axial placement study showed that with SB place at 35 percent passage the rotor produced the best results. For this configuration, the predicted peak total-to-total pressure ratio was 2.12 and the predicted peak total-to-total isentropic efficiency was 85.3 percent. The mass flow rate range, Equation (2), was 23 percent.

$$Mass-Flow-Rate-Range = \frac{\dot{m}_{max} - \dot{m}_{min}}{\dot{m}_{max}} \quad (2)$$

where the minimum and maximum mass flow rates were taken from a single speed line as shown in Fig 20.

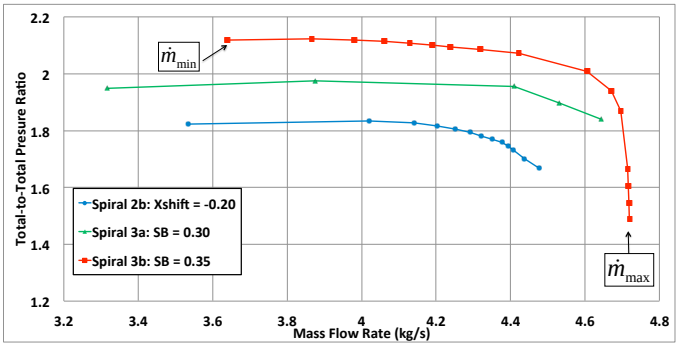

Fig. 20, TASR Spiral 3: Total-to-total pressure ratio map.

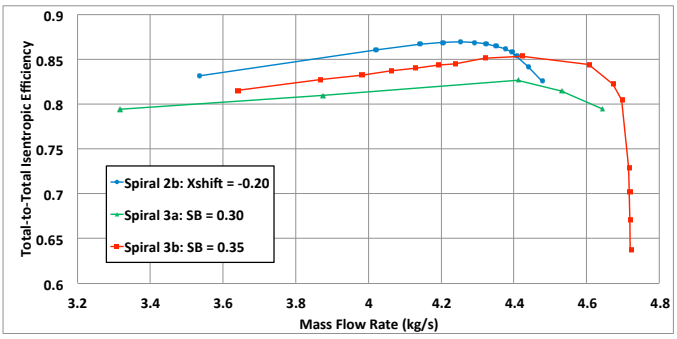

Fig. 21, TASR Spiral 3: Isentropic efficiency map.

A detailed structural analysis was performed on the final blade shapes that were designed during Spiral 3 and slight geometric adjustment had to be made to reduce the stresses at the root of the blades due to centrifugal forces at 30,000 rpm. This was the anticipated maximum speed during stall tests when the rotor would overspeed due to a constant power turbine drive. Full details of the analysis are given in [15]. The final rotor blisk is shown in Fig 22, including the shaft mounting holes and blade-to-disk fillets. The final machined part is shown in Fig 23.

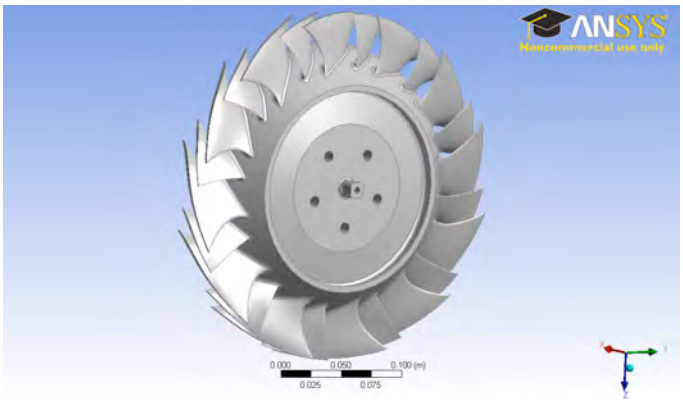

Fig. 22, TASR Spiral 3 structural analysis solid model.


Fig. 23, Final machined TASR blisk

TRANSONIC COMPRESSOR RIG (TCR)

Compressor Installation and Instrumentation

Modifications were made to the rotor-only test section of the TCR to accommodate the TASR as shown schematically in Fig 24. Due to the axially segmented construction of the TCR, the TASR was easily accommodated into the rig with the exception of a wider (in the axial direction) inner ring of abradable rubber material to accommodate the longer chord of the TASR blades. After assembly the inlet instrumentation was located in axial segment 1 (AS1), the casing transient pressure instrumentation over the rotor were located in axial segment 2 (AS2), and the outlet instrumentation was located in axial segment 3 (AS3). The axial segments are show in Fig 25 and the installed TASR blisk in the TCR is shown in Fig 26.

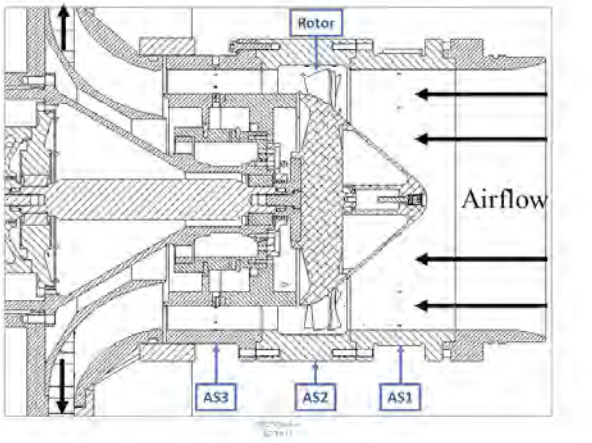

Fig. 24, TCR cross-section with the TASR installed.

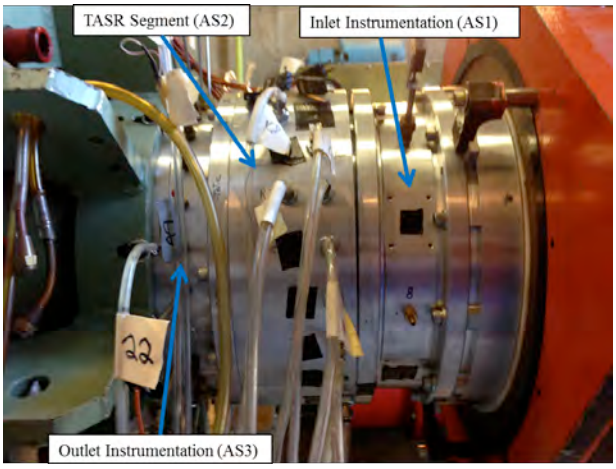

Fig. 25, TASR axially segmented casing.

Fig. 26, TASR blisk and hub section.

The TCR configuration and operation are described in detail by Grossman [10] and are summarized here. The TASR was powered by two opposed rotor, single stage air-operated drive turbines mounted on a common shaft as shown in Fig 27. The drive turbines received supply air from a 12-stage Allis-Chalmers axial compressor capable of providing 2.2 kg/sec mass flow rate at up to 2 atmospheres of gage pressure.

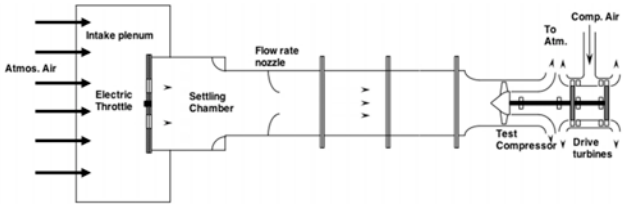

Fig. 27, Transonic Compressor Rig configuration

EXPERIMENTAL RESULTS

Prior to starting the experimental testing of the TASR installed in the TCR increased concern about the stability of the abradable strip material installed in the casing in the blade tip region necessitated the machining of the abradable material to expand the cold-shape tip gap from the planned 0.51 mm (0.020 in) to 0.91 mm (0.036 in). It was predicted that this would negatively impact the experimentally measured performance of the TASR, but the tradeoff was accepted to ensure the integrity of the TASR blisk.

Performance of the TASR was measured at 60 percent, 70 percent, 90 percent, 95 percent, and 100 percent of the 27,000 design speed. The total-to-total pressure ratio, total-to-total isentropic efficiency, and referred power were plotted versus mass flow rate for each specific test speed. From an experimental error analysis the greatest source of error was the mass flow instrumentation equating to a two percent error in the measured mass flow rate. The total-to-total pressure ratio versus mass flow rate is shown in Fig 28. This figure shows the characteristic increase of pressure ratio as the mass flow rate is decreased as a constant rotational speed. The compressor was throttled to stall for all speeds. At 100 percent design speed, the measured peak pressure ratio was 1.69 and mass flow rate range was 7.5 percent. At 70 percent design speed, the measure peak pressure ratio was 1.33 and the mass flow rate range was 18 percent.

Before proceeding with the comparison, it is important to recall that the numerically derived predicted performance was modeled using a TG of 0.25 mm (0.010 in) but the TASR was experimentally tested with a cold, non-deformed shape TG of 0.91 mm (0.036 in). Additionally, the numerical simulations performed in this study were predictive and time did not permit refining the simulations to try to match the predicted numerical performance to the measured experimental performance. As predicted, with a larger TG, the experimental data shows a reduced peak pressure ratio and increased mass flow rate at all operating speeds. At 100 percent design speed the predicted peak pressure ratio was 1.92, but the measured peak pressure ratio was 1.69. The predicted mass flow range was 6.0 percent and the measured mass flow range was 7.5 percent. Although the measured pressure ratio was lower than predicted the measured flow range was higher than predicted. This increased flow range will result in an increased operability range if used in an actual engine.

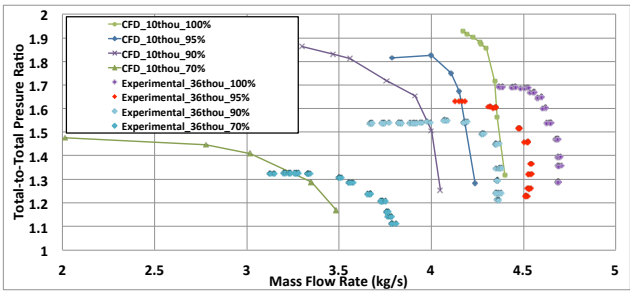

Fig. 28, TASR experimentally versus numerically determined total-to-total pressure ratio map.

Fig 29 shows the numerical results for total-to-total isentropic efficiency plotted on the map of the experimentally determined data. Again, the larger TG reduced performance and reduced the peak efficiency at all operating speeds but increased mass flow rate. The predicted peak efficiency for 100 percent design speed was 80 percent but the measured efficiency was 72 percent. Again, the experimental performance maps and the numerically determined maps matched in characteristic, in that although the pressure ratio and

efficiency were down due to the increased tip leakage the flow range was similar. The experimental flow range (at 0.91 mm tip gap) was slightly larger than that predicted at the analyzed 0.25 mm (0.010 in) tip clearance.

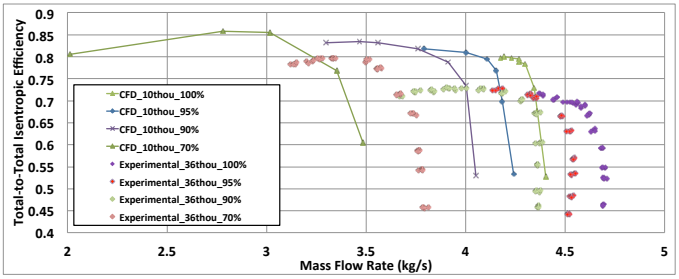

Fig. 29, TASR experimentally versus numerically determined isentropic efficiency map.

The power absorbed by the compressor versus mass flow rate for the range of operating speeds is shown in Fig 30. This is the corrected mass flow rate and it should be noted that the actual power absorbed by the TASR was less due to the upstream throttling. The peak power actually absorbed by the compressor at each operating speed is lower than presented. For example, at 100% design speed the measured corrected peak power absorbed was 425 kW. The measured uncorrected peak power absorbed was 317 kW. The corrected power was calculated using equation (3). The map for each operating speed is shifted to a higher mass flow rate range as predicted due to the increase in TG.

$$HP_C = C_p \dot{m} \left(T_{03} - T_{01} \right) \qquad (3)$$

where C_p is the specific heat of the air and $\dot{m}$ is the corrected mass flow rate.

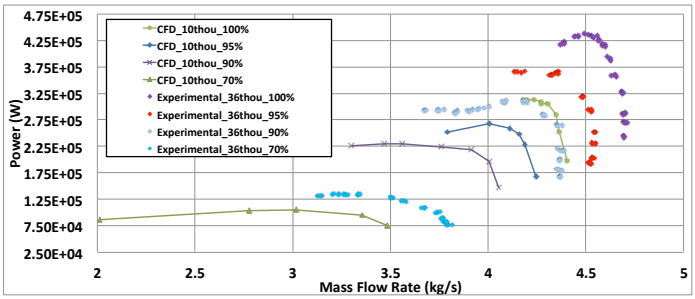

Fig. 30, TASR experimentally versus numerically determined power map.

Utilizing the MATLAB code developed by Londono [16] the unsteady Kulite data of the casing pressures was analyzed for the 100 percent design speed at the near-stall condition resulting in the contour plot shown in Fig 31. In this figure a strong oblique shock is originating from the leading edge (LE) of the splitter blade (SB) and a weaker oblique shock is originating from the LE of the main blade (MB). The casing contour plot extracted from the numerically derived performance data at 100 percent design speed in the near stall condition is also shown.

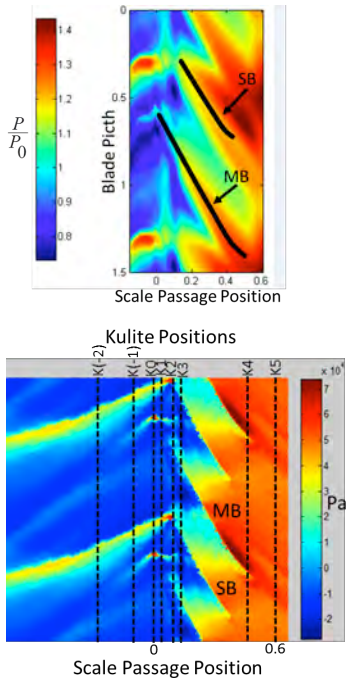

Fig. 31, TASR 100 % speed near-stall experimental (left) and computational (right) casing contour pressure plot.

Comparing these figures the experimentally derived contour plot for the same conditions shows similar flow field characteristics to the computational results. A strong oblique passage shock wave can clearly be seen starting in the SB LE tip region and a smaller oblique shock can be seen originating from the MB LE tip region. The combination of these shock waves inhibits the fluid flow creating flow blockage into the passage and setting up a stall condition.

CONCLUSIONS

The goal of this study was to design, test, and evaluate a transonic axial compressor rotor with splitter blades and all objectives were met. In accomplishing these objectives, several outcomes have been achieved:

1. A new design procedure has been developed and documented that uses commercial-off-the-shelf software for the geometric rendering and analysis of a transonic compressor rotor.
2. MATLAB was used to script the whole design procedure by performing a preliminary tip section design, defining blade parameters, and controlling both SolidWorks and ANSYS-CFX.
3. During a design cycle a complete constant speedline of the compressor was analyzed from open

throttle (choke) to stall conditions. This allowed overall performance to be evaluated and compared during each cycle.

4. After restacking of the blade profiles and including fillet radii at the blade roots the design was frozen. A solid blisk (blade and disk) was machined out of 7075-T6 aluminum alloy and tested in the Transonic Compressor Rig.

5. This study advanced the understanding of splitter blade geometry, placement, and performance benefits. In particular, it was determined that moving the splitter blade forward in the passage between the main blades, which was a departure from the trends demonstrated in the few available previous transonic axial compressor splitter blade studies, increased the mass flow range with no loss in overall performance.

6. With a large 0.91 mm (0.036 in) tip clearance, to preserve the integrity of the rotor, the experimentally measured peak total-to-total pressure ratio was 1.69 and the peak total-to-total isentropic efficiency was 72 percent at 100 percent design speed. Additionally, a higher than predicted 7.5 percent mass flow rate range was experimentally measured, which would make for easier engine control if this concept were to be included in an actual gas turbine engine.

ACKNOWLEDGMENTS

This project was performed as part of the Army Research Office funded project on, "Understanding and Mitigating Vortex-Dominated, Tip-Leakage and End-Wall Losses in a Transonic Splittered Rotor Stage." Project no. 60039EG. The support of technical monitor Dr. Frederick Ferguson is greatly appreciated.

REFERENCES

1. Wennerstrom, A. J., *Design of Highly Loaded Axial-Flow Fans and Compressors*, White River Junction, VT: Concepts ETI, Inc., 2000, p. 69.

2. Wennerstrom, A. J., "Some Experiments with a Supersonic Axial Compressor Stage," ASME Journal of Turbomachinery, vol. 109, pp. 388–397, 1987.

3. Wennerstrom, A. and Hearsey, R., "The Design of an Axial Compressor Stage for a Total Pressure Ratio of 3 to 1," Aerospace Research Laboratories report AR 71-0061, Wright-Patterson AFB, Dayton, Ohio, 1971.

4. Wennerstrom, A. J. and Frost, G., "Design of a Rotor Incorporating Splitter Vanes for a High Pressure Ratio Supersonic Axial Compressor Stage," Aerospace Research Laboratories report AR 74-0110, Wright-Patterson AFB, Dayton, Ohio, 1974.

5. Wennerstrom, A., Buzzel, W. and Frost, G., "Test of a Supersonic Axial Compressor Stage Incorporating Splitter Vanes in the Rotor," Aerospace Research Laboratories report AR 75-0165, Wright-Patterson AFB, Dayton, Ohio, 1975.

6. Tzuoo, K. L., Hingorani, S. S. and Sehra, A.K., "Design Methodology For Splittered Axial Compressor Rotors," in *Gas Turbine and Aeroengine Congress and Exposition*, Brussels, Belgium, 1990.

7. McClumphy, J., "Numerical Investigation Of Subsonic Axial-Flow Tandem Airfoils For A Core Compressor Rotor," Ph.D. dissertation, Dept. Mech. Eng., Virginia Polytechnic Institute and State University, Blacksburg, VA, 2008.

8. Sanger, N. L., "Design Of A Low Aspect Ratio Transonic Compressor Stage Using CFD Techniques," *ASME Journal of Turbomachinery*, vol. 118, pp. 479–491, 1996.

9. Sanger, N. L., "Design Methodology For The NPS Transonic Compressor," Turbopropulsion Laboratory, Naval Postgraduate School, Monterey, CA, Tech. Note 99–01, Aug. 1999.

10. Grossman, B. L., "Testing And Analysis Of A Transonic Axial Compressor," M.S. Thesis, Dept. Aeronautical and Astronautical Eng, Naval Postgraduate School, Monterey CA, 1997.

11. Boyter, R. A., "Computational Fluid Dynamic Simulation Of Transonic Compressor Fan Performance," M.S. Thesis, Dept. Mechanical and Aerospace Eng, Naval Postgraduate School, Monterey, CA, 2010.

12. McNab, D. J., "Experimental Testing And CFD Modeling Of An Advanced Transonic Compressor For Military Applications," M.S. Thesis, Dept. Mechanical and Aerospace Eng, Naval Postgraduate School, Monterey CA, 2011.

13. Drayton, S., "TPL Transonic Axial Compressor Rotor Design Tool Software," Turbopropulsion Laboratory, Naval Postgraduate School, Monterey, CA, Tech. Note 13–01, Sep. 2013.

14. Sommer III, H. J., (2002, May 14). *Polygeom.m* [Online]. Available http://www.me.psu.edu/sommer/

15. Drayton, S., “Design, Test and Evaluation of a Transonic Axial Compressor Rotor with Splitter Blades,” PhD Dissertation, Dept of Mechanical and Aerospace Engineering, Naval Postgraduate School, Monterey CA, 2013.

16. Londono, A., “Near-stall modal disturbances within a transonic compressor rotor,” M.S. thesis, Dept. Mechanical and Aerospace Eng, Naval Postgraduate School, Monterey CA, 2011.